Chapter 10

Review on Creep Analysis and Solved Problems

Vahid Monfared

Additional information is available at the end of the chapter

http://dx.doi.org/10.5772/intechopen.71184

Abstract

This chapter presents a useful literature reviews and applied solved problems that focus on the creep phenomenon and behavior of it in the solids. Various insights and available studies are reviewed and investigated regarding the creep behavior analysis in three categories such as analytical, numerical and experimental methods. In addition, novel and recent findings are presented in this chapter such as predicting and obtaining the viscosity of the solids at high temperatures using steady state creep phenomenon (i.e., introducing a simulation and analogy between creeping solids and viscous fluids).

Keywords: creep, analytical, numerical, experimental methods, solved problems

1. Introduction

Creep is a slow, continuous deformation of a material under constant stress and temperature. On the other hand, creep phenomenon in solids under high stress and temperature is one of the important topics in the scientific societies, and therefore, the creep analysis become more significant in various industries. Therefore, study on the process of the creep phenomena is essential and significant for engineering applications concerning high temperature and high stress. For instance, spaceships, turbine blades and discs are commonly under the creep effects. Additionally, predicting the creep behavior is very important for designing the advanced reinforced/nonreinforced materials. Consequently, a logical analysis of the creep behavior and its mechanisms for these materials is crucial. Creep phenomenon may be happened in short fiber composites or nanocomposites because of any elevated temperatures and applied loads which can be dangerous for composites and structures. Therefore, a thorough knowledge of creep characteristics and deformation mechanisms of reinforced and nonreinforced materials is required to utilize these composites in high stress and high temperature applications. In recent years, extensive investigations have been conducted to predict the steady state creep behaviors of the materials (see **Figure 1**).

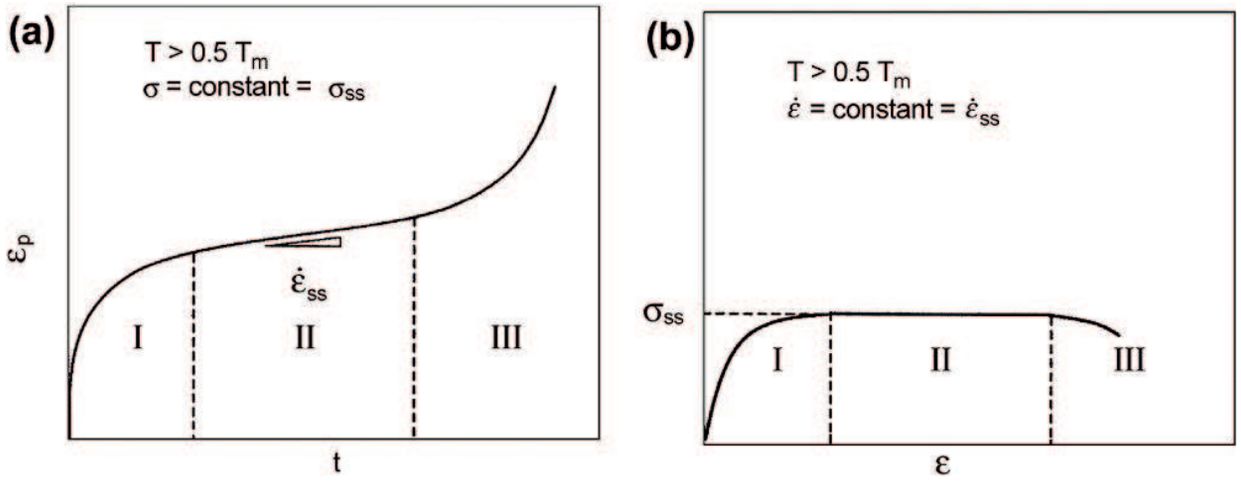

Figure 1. (a) Creep $\varepsilon - t$ diagram (b) creep $\sigma - \varepsilon$ diagram [105].

These advanced materials are generally used in various industries such as aircraft and aerospace industries and other engineering applications because of numerous advantages. One of the hazardous phenomena is creep occurrence which may occur in these materials. Consequently, the creep must be accurately studied and analyzed to prevent unsafe and undesired events. Several investigations have been performed to predict the creep behaviors of the advanced reinforced/nonreinforced materials. In this chapter, in addition to presenting some insights, the related previous studies are reviewed in three categories such as analytical, numerical and experimental methods.

2. Analytical methods

In reinforced materials, various theoretical studies are based on the shear-lag theory [1–13]. For more illustrations, 1D shear-lag theory was initially proposed by Cox [1], which is a strong model for the stress transfer analysis of the unidirectional fibrous composites. Recently, Mondali et al. [12] introduced a theoretical approach to predict the second-stage creep behavior of the short fiber composites by using shear-lag model and imaginary fiber method. The creep behavior of the creeping matrix was predicted using a creep exponential law. Moreover, various investigators have studied fibrous composites by employing imaginary fiber method and technique (fictitious fiber) elastically [14–18].

For instance, one of the useful and valuable researches was done by Weng and Sun [14]. They employed the fictitious fiber technique and method to study the effects of the fiber length on elastic moduli of randomly oriented chopped-fiber composites theoretically. The method and technique is analogous to the imaginary fiber technique to analyze the short fiber composites. The mentioned solution method based on fictitious fiber technique [14] is similar to Hsueh's elastic solution [15], known as the imaginary fiber technique. The scientific application of the fictitious and imaginary fiber method is very significant for analyzing the matrix located at the top of the fiber. In addition, this model may assist to the analysis of a full and complete fibrous composite.

Stress transfer from the matrix to the embedded fiber in fiber-reinforced composites has been studied elastically while the loading direction is parallel to the fiber axis and the fiber is bonded to the matrix. Stress transfer occurs both at the interface along the fiber length and at the ends of the fiber. Nevertheless, the boundary condition at the bonded ends is unclear, and different suppositions were made analytically to achieve solutions for this stress transfer problem. To this end, a novel insight of supposing imaginary fibers in the fibrous composite was introduced. In comparison to the prior theoretical solutions, this method [15] bears more physical meaning and is in better agreement with numerical (FEM) and experimental results [15].

In addition, many investigations were carried out concerning the creep of the fibrous composites and applications by different methods theoretically [19–24]. Some investigators have employed different methods in place of the shear-lag model to solve the problems like Eshelby's thought experiment with a formulation based on the Schapery model [19] and variational approach [21]. Also, Monfared et al. [22] proposed the second-stage creep strain rate of the short fiber composites without utilizing the shear-lag theory. They determined various key unknowns in the steady state creep of the short fiber composites using mapping function and dimensionless parameter techniques.

Furthermore, novel theoretical insight and formulation have been proposed for studying the second-stage creep in fibrous composites utilizing complex variable method, at which, both the matrix and fiber creep at low stresses and temperatures. To study the creeping fiber, a plane stress model has been employed. Significant novelties of the research work of Monfared et al. [23] are determination of the displacement rates with suitable boundary conditions in the creeping fibers and also utilizing the complex variable method in the creep analyzing. It is important that the model and method may be helpful to investigate the creep behavior in polymeric matrix composites. Furthermore, another major application of the method is to theoretically analyze the creep or elastic behavior of carbon nanotube polymer composites. Here, as an example, a result presented in Ref. [23] is introduced as the following:

$$\dot{u}_1(z,\overline{z}) = \varphi(z) + \Psi(z - \lambda\overline{z}) \tag{1}$$

$$\dot{u}_2(z,\overline{z}) = \mu\left[\oint_c 2\aleph\left(\frac{5z-\lambda\overline{z}}{4}\right)dz - \oint_c \lambda\aleph\left(\frac{5z-\lambda\overline{z}}{4}\right)d\overline{z}\right] + \rho\left(\frac{z}{2}+\frac{5}{6}\overline{z}\right) \tag{2}$$

λ is equal to $\frac{5}{3}$ obtained by solving the partial equations, μ is equal to $\frac{1}{3}$ and c is closed finite region in steady state creep. Using the residual theorems in complex variable analysis, gives

$$\oint_c \aleph(z,\overline{z})d(z,\overline{z}) = 2\pi i Res\ \aleph(z,\overline{z})\Big|_{z,\overline{z}=z_0} \tag{3}$$

In above equation, *Res* indicates the residual value of $\aleph(z,\overline{z})$. Moreover, two analytical functions ρ *and* $\aleph$ are introduced through Cauchy-Goursat theorem. Therefore, $\dot{u}_1, \dot{u}_2, U$ and $\overline{U}$ may be obtained utilizing complex variable in the second-stage creep of the fibrous composites. All the mentioned theoretical and analytical functions like $\varphi(z)$ can be supposed by a polynomial function of degree n with its unknown coefficients. The unknowns may be obtained

employing the appropriate boundary conditions. As the major benefit of the method and formulation of [23], Eq. (3) will be able to analyze and solve the improper integrals [23]. Moreover, displacement rates $\dot{w}_1$ and $\dot{w}_2$ are obtained utilizing different boundary conditions in the crept matrix, distinctive geometric relations and same procedures. That is, $\dot{w}_1 = \beth(z) + \Lambda(z - \overline{z}) = \Upsilon(z - \overline{z})$ and $\dot{w}_2 = \left[\oint_c 2\mathcal{L}(z - \overline{z})dz - \oint_c \mathrm{T}\mathcal{L}(z - \overline{z})d\overline{z}\right]\mathcal{B} + \mathfrak{O}(z + \overline{z}) = \mathcal{G}(\overline{z} + z)$. Using the boundary conditions, displacement rates $\dot{u}_1, \dot{u}_2$ and $\dot{w}_1, \dot{w}_2$ are coupled simultaneously. In above equations, (u_1, u_2) and (w_1, w_2) are displacement fields in the fiber and matrix, respectively. Also, subscripts 1 and 2 are related to x_1 and x_2 directions [23].

3. Numerical methods

Numerical attempts have been made for analyzing the creep problems by various investigators. Numerical methods have helped the researchers for analyzing the problems [25–33]. The purpose of the paper [30] is to obtain the general creep mechanisms for the fibrous composites (MMCs) subjected to axial stress states and to build a relation between the macroscopic stable creep behavior and the material micro-geometric parameters numerically. The unit cell models have been employed to compute the macroscopic creep behavior with different micro-geometric parameters of the fibers on different loading directions. The influence of the geometric parameters of the fibers and loading directions on the macroscopic creep behavior was determined previously. The matrix and fiber interface were considered by a third layer, matrix and fiber interlayer, in the unit cells with different creep properties and thickness. Based on the numerical-obtained results of the unit cell models, a statistic model was introduced for the plane randomly distributed-fiber MMCs. The fiber breakage was taken into account in the statistic model because it starts early in the creep life experimentally. With the distribution of the geometric parameters of the fibers, the obtained results of the statistic model agree well with the experiments. With the statistic model, the influence of the geometric parameters and the breakage of the fibers in addition to the properties and thickness of the interlayer on the macroscopic steady state creep rate were discussed [30].

FEM investigation for steady state creep behavior of the creeping metal matrix composite was done with supposing the fiber-matrix debonding parameter in the modeling by Mondali et al. [31]. Accuracy of simulation and being time consuming are several major difficulties of FEM generally. In addition, one of the significant sections of reference [33] is to predict the limited creep debonding at the interface in the second-stage creep of the fibrous composites subjected to axial stress. At this point, a key formulation, presented in Ref. [33], is generally introduced as the following:

The average axial stress of fiber is semi-analytically obtained as a function of interfacial shear stress which is presented as follows:

$$\overline{\sigma}_{zz}^{f} = \Gamma \times \tau_i \times \left(\mathbb{Z}l^{\delta}D^{-\delta} - \mathbb{C}z^{\delta}D^{-\delta}\right) \tag{4}$$

where parameters Γ, $\mathbb{Z}$ and $\mathbb{C}$ are constant coefficients and also τ_i and $\overline{\sigma}_{zz}^{f}$ are the interfacial shear stress and the average axial stress of the elastic fiber, respectively. In addition, the parameters of

$l^{\delta}D^{-\delta}$ and $z^{\delta}D^{-\delta}$ are dimensionless parameters, which are employed to determine the quasi shear lag formulation, that is, Eq. (4). Recent formulation may be obtained using linear combination of the elastic fiber diameter ($D = 2a$), axial position (z), dimensionless parameters (lD^{-1}, zD^{-1}) and the fiber length (l) considering semi-theoretical approaches. After determining the unknown coefficients, QSL formulation will be determined as below:

$$\overline{\sigma}_{zz}^{f} \cong \tau_i|_{z=l}^{r=a} \times \left(\frac{54l - 35z}{10D}\right) \tag{5}$$

where $\tau_i|_{z=l}^{r=a}$ is the maximum value of shear stress along the fiber length at the interface (i.e., at $z = l, r = a$). Note that the formulation of interfacial shear stress, i.e. τ_i, is proposed by Monfared et al. [22], which has been used for determining average axial stress in the fiber $\overline{\sigma}_{zz}^{f}$ as follows [22]:

$$\tau_i(z) = \frac{\eta}{\sqrt{3}} \ln\left(1 + \frac{\sqrt{3}C}{\eta} z\right) \tag{6}$$

In which,

$$C = \exp\left(\frac{\sqrt{3}}{\eta}\tau_i\right)\frac{d\tau_i}{dz} \tag{7}$$

Other relation for obtaining a shear stress at the interface has the following form [22]:

$$\tau_i = \tau_{\mathrm{rz}}^{\mathrm{m}}\big|_{r=a} = \underset{(\mathrm{r,z})\to(\mu,\aleph)}{limit}\left[\frac{\eta \ln\left(\frac{\dot{\varepsilon}_{eq}}{\lambda}\right)\dot{\gamma}_{\mathrm{rz}}}{3\dot{\varepsilon}_{eq}}\right]_{r=a} \tag{8}$$

In which,

$$\dot{\gamma}_{rz} = \frac{\partial \dot{u}}{\partial z} + \frac{\partial \dot{w}}{\partial r} = 2\dot{\varepsilon}_{rz} \tag{9}$$

where $\mu = [\mathrm{a,b}], \aleph = (0, l]$, which imply $a \le \mu \le b$ and $0 < \aleph \le l$. Also, $\dot{\gamma}_{\mathrm{rz}}$ is the shear strain rate in the direction indicated by its subscript and $\dot{u}$ and $\dot{w}$ are, respectively, the radial and axial displacement rates.

On the other hand, the average axial stress in the fiber is approximately linear in elastic state, that is, $\overline{\sigma}_{zz}^{f} \cong g_1 z + g_2$. Note that the unknown coefficients g_1 and g_2 are obtained employing mentioned calculations and engineering estimations. In general, average axial stress in the fiber is calculated using maximum shear stress at the interface and geometric factors. As mentioned earlier, a weight coefficient is considered for any parameter such as g_1 and g_2 with parameter z employing numerical methods, weighted calculus (computer coding) and meta-calculus with considering nonlinear regression and neural network approaches [33].

4. Experimental methods

Unlike several difficulties of the experimental methods such as complexity of them (they may be time-consuming, expensive and intricate), they are useful to predict the steady state creep behaviors [34–49]. For instance, the second-stage creep behavior of the composite "SiC/Al6061" was experimentally and analytically analyzed by Morimoto et al. [36], in which happening of the non-aligned fibers and creation of the microcracks in the creeping composite are some difficulties during the experimental process. For more illustration, the creep behavior of the TiC-particulate-reinforced Ti alloy composite was studied at temperatures from 500 to 650°C and applied stresses from 230 to 430 MPa [37].

The steady state creep behavior of poly (vinylidene fluoride) (PVDF)/multiwall carbon nanotubes nanocomposites was investigated at various stress levels and temperatures experimentally. To fine-tune the ability to transfer stress from matrix to carbon nanotubes, bud-branched nanotubes were fabricated. The PVDF showed improved creep resistance by adding carbon nanotubes. However, bud-branched nanotubes showed a modified stress- and temperature-dependent creep resistance in comparison with carbon nanotubes. Also, at low stress levels and low temperatures, bud-branched nanotubes showed better improvement of the creep resistance than that of virgin carbon nanotubes, whereas at high stress levels and high temperatures, the virgin carbon nanotubes presented better creep resistance than that of bud-branched nanotubes. Differential scanning calorimetry (DSC), WAXD and Fourier transform infrared spectroscopy (FTIR) were used to characterize the crystalline structures, and dynamic mechanical properties were characterized by dynamic mechanical analysis (DMA) testing. The Burger's model and the Findley power law were utilized to model the creep behavior, and both were found to well describe the creep behavior of PVDF and its nanocomposites. The relationship between the structures and properties was analyzed based on the parameters of the modeling. The improved creep resistance for PVDF by adding the nanotubes would be beneficial for its application in thermoset composite welding technology [47].

The high-temperature creep behaviors of 7075 and 2124 aluminum alloys have been analyzed by the constant-stress uniaxial tensile creep experiments. In addition, constitutive models for describing the high-temperature creep behaviors of the studied aluminum alloys were established based on the continuum damage mechanics (CDM). Initially, the continuum damage mechanics (CDM) models were simplified to explain the primary and secondary creep of 7075 aluminum alloy. Then, because the effects of the applied stress on the creep damage during tertiary stage were not entirely considered in the original CDM model, the modified constitutive models were presented to predict the creep-rupture behavior of 2124 aluminum alloy. A stress exponent D, which can preferably reveal the effects of the applied stress on the stationary creep damage, was presented in the modified model. The results of this investigation showed that a good agreement between the measured and predicted results was determined, which confirms that the established creep constitutive models can give an precise and exact approximation of the high-temperature creep behaviors for 7075 and 2124 aluminum alloys [48]. Briefly, the high-temperature creep behaviors of 7075 and 2124 Al alloys were investigated; a stress exponent was proposed to preferably reveal the

effects of the stress on creep damage and the established CDM models correlate well with the experimental results [48].

In addition, the second-stage creep and recovery behaviors of polystyrene composites filled with 2D chemically diminished graphene oxide sheets have been investigated, in which a series of stationary creep and recovery characterization tests have been carried out for thermoplastic composites filled with three different types of carbon nanoadditives (including CB, CNT and graphene). Furthermore, the thermal and dynamic mechanical properties of the composites have been studied and analyzed to find and understand the relative formation mechanisms generally [49].

5. Complementary methods

Complementary methods may be a combination of the three mentioned methods of analytical, numerical and experimental approaches such as semi-analytical methods or other supplementary approaches. The mentioned methods (complementary methods) are a supplementary for the three mentioned methods (analytical, numerical and experimental methods).

A semi-analytical formulation has been presented for obtaining the viscosity of solids (such as metals) using the steady state creep model of the short fiber composites. For achieving this aim, fluid mechanics theory was used for determining the viscosity. Sometimes, obtaining the viscosity is experimentally difficult and intricate. Therefore, the present model may be beneficial to obtain the viscosity of the metals [50].

Another research work was presented for simple and fast estimation of the creep plastic behavior of the short fiber composites by a new approach based on neural network prediction. The method has been introduced to diminish the solution process. Furthermore, as an important application of the approach and the model mentioned in Ref. [51], spaceships and turbine blades are commonly under the stationary creep effects. Thus, analysis of the steady state creep is necessary and essential in various industries. Therefore, analysis of the second-stage creep behavior is mandatory for analysis of failure and fracture and creep resistance of the fibrous composites. One of the major applications of the research work [51] is the design of the fibrous composites with optical fibers and devices [51].

A new analytical approach was presented for analyzing the steady state creep in a short fiber composite SiC/Al6061 (Silicon Carbide/Aluminum 6061) under axial load based on high order displacement functions. The creep behavior of the matrix was described by an exponential law with elastic behavior of fibers. Predicting the creep behavior of the short fiber composite "Silicon Carbide/Aluminum 6061" using high order functions analytically was the novelty of the work. The research work was presented in order to prevent unwanted happenings, in addition to the control of the second-stage creep deformation rate. As a result, the creep behaviors are controllable, and the diagrams have smooth gradients and slopes [52]. Indentation creep behavior at room temperature and its mechanism of Ti-10 V-2Fe-3Al alloy with dual phase structure were investigated. Micro-indentation creep tests were performed under the maximum indenter load ranging from 1500 to 4500 mN and the holding time of 300 s. The

effect of indenter load on creep behavior and creep parameters, like creep rate, creep strain rate, indentation stress and creep stress exponent, were analyzed at the steady state creep. The results revealed that creep parameters exhibited significantly indentation depth dependent. At the secondary stage of creep, creep strain rate and creep rate increased with the increase of maximum indenter load, whereas creep stress and creep stress exponent exhibited an opposite trend. Especially, creep stress exponent of 7.65 ± 1.25 in power-law creep behavior of Ti-10 V-2Fe-3Al alloy, which was consistent with dislocation process, indicated that the secondary stage of creep may be dominated by dislocation climb. Furthermore, experimental data and figures were used to evaluate and comprehend likely creep mechanisms during a micro-indentation scheme of Ti-10 V-2Fe-3Al alloy [53]. Briefly, micro-indentation creep behavior with various indenter loads was investigated; creep rate and indentation stress showed a linear relationship with indenter loads; high creep strain rate can be induced by increasing indenter load at holding time; indenter load effects on creep stress exponent are similar to that of hardness and the creep behavior at secondary stage may be dominated by dislocation climb [53].

Steady state creep was characterized for Ni-8YSZ solid oxide fuel/electrolysis cell (SOFC/SOEC) substrate material. Intrinsic and extrinsic factors affecting creep behaviors such as compositional ratio, porosity and mechanical loading configuration were assessed. Mechanical tests were supported by analytical and numerical calculations. The results indicated a diffusion-dominated creep mechanism under both compressive and tensile creep conditions. Creep appeared to be dominated by the ceramic phase. Porosity significantly reduced creep resistance. The activation energy was discussed based on loading configuration, temperature and porosity [54]. In brief, the creep of porous Ni-8YSZ anode substrates was investigated systematically; the porosity, composition ratio and loading configuration have effects on creep; the suitability of different testing methods was successfully analyzed and derived creep parameters can be used for materials' validation and modeling [54].

Creep deformation and fracture behaviors of Sanicro 25 alloy were obtained based on long-term creep strain tests. The multiscale precipitation behaviors were calculated thermodynamically and inspected by examination of the microstructure of the as-crept alloy [55]. Briefly, multiscale precipitation behaviors of Sanicro 25 during long-term creep were revealed; fine-distributed nanoscale precipitates were found as the main strengthening phases of Sanicro 25 at elevated temperatures and preferred grain orientation of Sanicro 25 before and after creep under different conditions were investigated by electron back-scattered diffraction [55]. *In situ* neutron diffraction measurements were performed on monocrystalline samples of the Ni-based superalloy CMSX-4 during N-type γ' raft formation under the tensile creep conditions of 1150°C/100 MPa and subsequently on a rafted sample under the low temperature/high stress creep conditions of 715°C/825 MPa.

During 1150°C/100 MPa creep, the γ' volume fraction decreased from ~70 to ~50%, the lattice parameter misfit was partly relieved and the load was transferred from the creeping γ matrix to the γ' precipitates. In the process of cooling back to room temperature, a fine distribution of γ' precipitates formed in the γ channels, and these precipitates were present in the 715°C/825 MPa creep regime. Under low temperature/high stress creep, the alloy with rafted γ'

microstructure exhibited superior creep strength to the cuboidal γ' microstructure produced following a standard heat treatment. A lengthy creep incubation period was observed, believed to be associated with {111} ⟨110⟩ dislocations hindering propagation of {111} ⟨112⟩ dislocations. Following the creep incubation period, extensive macroscopic creep strain accumulated during primary creep as the γ-phase yielded. Finally, the diffraction data suggest a loss of precipitate/matrix coherency in the (0 k0) interfaces as creep strain accumulated [56]. Bending creep deformation mechanism for nickel nanobeam was investigated using molecular dynamics simulation. Low temperature creep deformation ($T < 0.3T_m$) was found to be guided by jog formation and glide motion of grain boundary, whereas lattice diffusion, grain boundary migration and sliding are the controlling mechanism for high-temperature deformation ($T > 0.5T_m$). The occurrence of tertiary creep regime was observed only at high-temperature deformation due to creep instability caused by cavity formation. It was revealed through dislocation analysis that intrinsic Frank partial dislocations are the driving factor for cavity generation leading to intergranular fracture [57]. Briefly, it is for the first time, the study of bending creep deformation and the underlying mechanism at nanoscale level; jog formation helps the grain boundary movement during low temperature bending creep deformation; intrinsic Frank dislocations cause cavity formation at tertiary regime for high-temperature bending creep [57].

The as-received cast and forged (C&F) P91 steel was subjected to the creep test at temperature of 620–650°C for applied stress of 120 MPa. The room temperature tensile test was conducted after normalizing and tempering (N&T) treatment of the ruptured creep specimen. The standard tensile test specimen was prepared from the gauge section of creep-ruptured specimen. The N&T treatment was performed to restore the microstructure and mechanical properties of virgin P91 steel (N&T P91 steel). The microstructure of creep-fractured specimen in ruptured state and N&T condition were characterized by using field-emission scanning electron microscope (FE-SEM) with energy dispersive X-ray spectroscopy (EDS). The fracture surface morphology of crept specimen and the tensile tested specimen was also studied. The effect of prior creep deformation on the mechanical strength was more significant in the sample with longer creep rupture life [58].

Briefly, creep test was performed in temperature range of 620–650°C and at stress of 120 MPa; the effect of creep rupture life on precipitate size and fraction area of precipitates; the effect of creep rupture life on fracture surface morphology of creep tested cast-forged P91 steel; the tensile properties of N&T creep fractured material compared with N&T cast-forged P91 steel and the fracture surface morphology of tensile fractured surface by using FESEM were studied [58] (see **Figures 2, 3**).

The creep behavior and microstructural evolution of 8030 alloy at 90–150°C and 50–90 MPa of applied tensile stress were investigated by creep testing and transmission electron microscopy. The 8030 alloy possesses excellent creep resistance at low temperatures. The sizes of a small number of subgrains increase during the creep process due to subgrain merging. A creep activation energy of 123.2 kJ/mol is close to that of the lattice self-diffusion in aluminum, implying that a lattice self-diffusion mechanism is dominant at 150°C/90 MPa (**Figures 4** and **5**), [59].

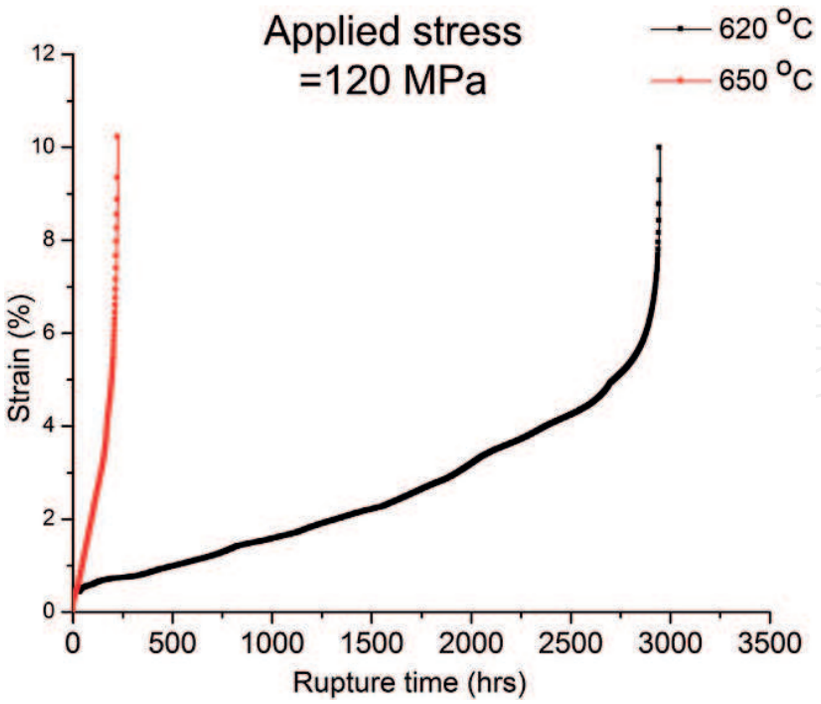

Figure 2. Creep rupture behavior of P91 steel [58].

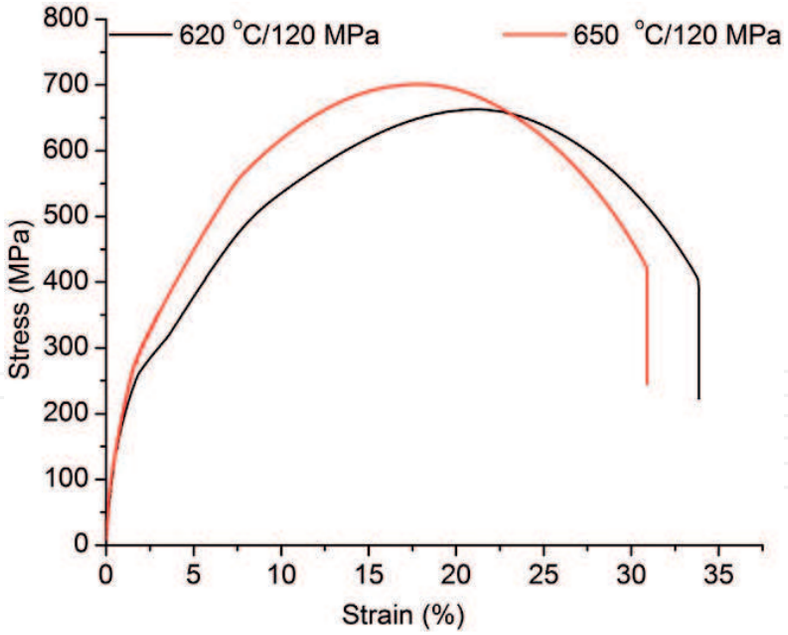

Figure 3. Engineering stress-strain curve [58].

Briefly, the 8030 alloy possesses excellent creep resistance at low temperatures; Al_3Fe-phase can improve the creep resistance of 8030 alloy; there are two kinds of creep mechanism at low temperature; the creep threshold stress is close to 0 MPa at 90 MPa/150°C [59].

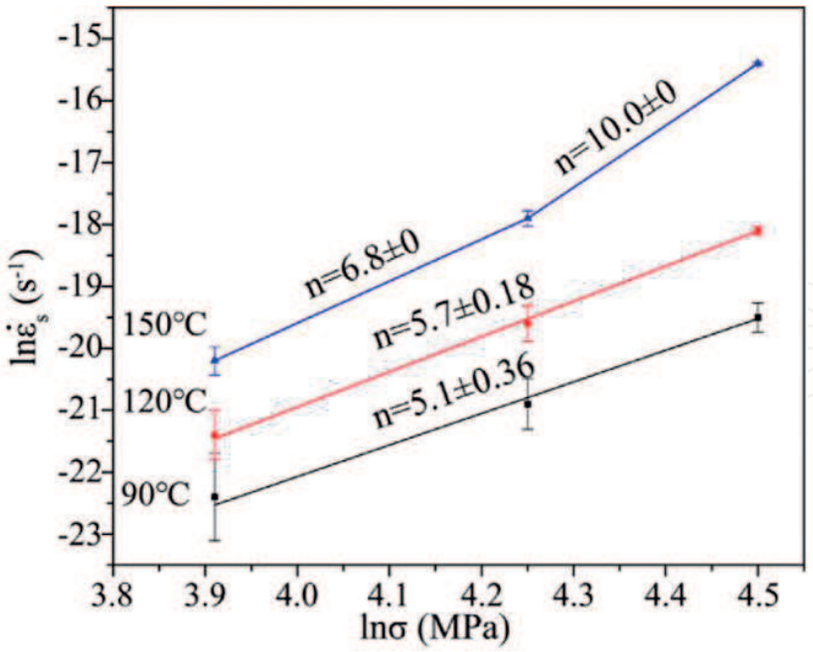

Figure 4. Relationship between ln $\dot{\varepsilon}_s$ and ln σ of 8030 alloys. (error bars: One standard deviation) [59].

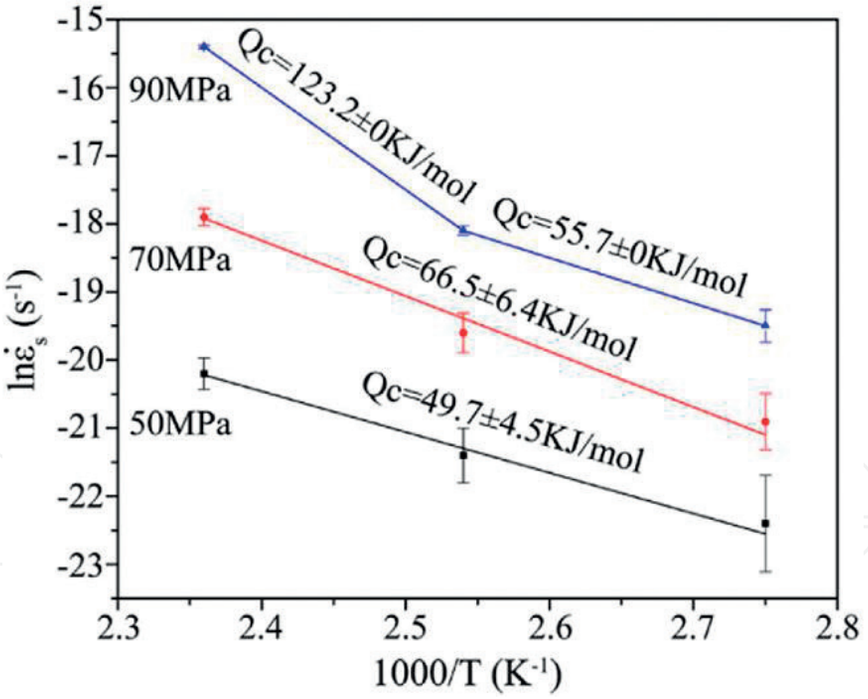

Figure 5. Relationship between ln $\dot{\varepsilon}_s$ and ln σ of 8030 alloys. (error bars: One standard deviation) [59].

Study of creep behavior of base metal (without weld) and welded specimens of P91B steel over a range of temperatures (600–650°C) and stresses (50–180 MPa) showed similar values of minimum creep rates for both specimens at higher stress regime (>100 MPa), whereas significantly higher creep rates in the case of welded specimens at lower stress regime. Considering

that welded specimen is composed of two distinct structural regimes, that is, weld-affected zone and base metal, a method has been proposed for estimating the material parameters describing creep behavior of those regimes.

Stress-strain distribution across welded specimen predicted from finite element analysis based on material parameters revealed preferential accumulation of stress and creep strain at the interface between weld zone and base metal (**Figures 6** and **7**). This is in agreement with the experimental finding that creep rupture preferentially occurs at intercritical heat-affected zone in welded specimens owing to ferrite-martensite structure with coarse $Cr_{23}C_6$ particles [60]. Briefly, comparison of creep properties of welded and virgin specimens of P91B steel was performed; at lower stresses (<100 MPa), welded samples show higher minimum creep rate; creep rupture at intercritical heat-affected zone (IC-HAZ) in welded specimens; FEA showing accumulation of creep strain in weld/base metal interface and precipitate-free soft ferrite matrix accumulates strain and weakens IC-HAZ [60].

A group of segmented polyurethane copolymers with different hard segment (HS) contents were successfully synthesized. The microstructure of the PU copolymers was characterized via Fourier transform infrared spectroscopy (FTIR), differential scanning calorimetry (DSC), dynamic mechanical analysis (DMA) and small-angle neutron scattering (SANS) [61]. The creep behaviors of two alloys were studied under the temperature of 700°C and three applied stresses (560, 650 and 720 MPa) in order to investigate the creep mechanisms of Inconel718 and Allvac718Plus, using multiple microstructural analysis methods, including scanning electron microscope (SEM), field-emission scanning electron microscope (FE-SEM) and transmission electron microscopy (TEM).

Result showed that steady state region is not observed in these two alloys. Creep curves of two alloys were composed of primary region and tertiary region. Tertiary region occupies a dominant position. Ductile dimples were observed on creep fracture surface, indicating creep mechanisms of two alloys are the formation of creep voids. Also, the formation of creep voids is found to be correlated with three factors which are dislocation multiplication, dislocation motion and dislocation obstacles. Inconel718 has higher dislocation multiplication rate, larger dislocation motion rate and more δ-phases and fewer bands than Allvac718Plus. Therefore, Inconel718 has higher creep voids rate than Allvac718Plus, leading to the result that Inconel718 has shorter creep life than Allvac718Plus [62].

A spark plasma sintering (SPS) apparatus was used to perform uniaxial compressive creep tests on dense SPS-processed fine-grained alumina (**Figure 8**). Experiments were carried out in the 1125–1250°C temperature range under an applied stress of 80–120 MPa. Creep rates, stress exponent and apparent activation energy were determined. The microstructure of deformed samples was characterized by HRSEM. The creep rates, stress exponent (1.9–2.1) and apparent activation energy (454 kJ/mol) values obtained are in a good agreement with data reported in the study regarding creep of fine-grained polycrystalline alumina. These results, together with microstructural observations, suggest that the creep mechanism involved was grain boundary sliding (GBS), accommodated by dislocation climb and controlled by diffusion along the grain boundaries. It was thus demonstrated that an SPS apparatus can be employed as an accurate high-temperature creep testing system [63].

http://dx.doi.org/10.5772/intechopen.71184

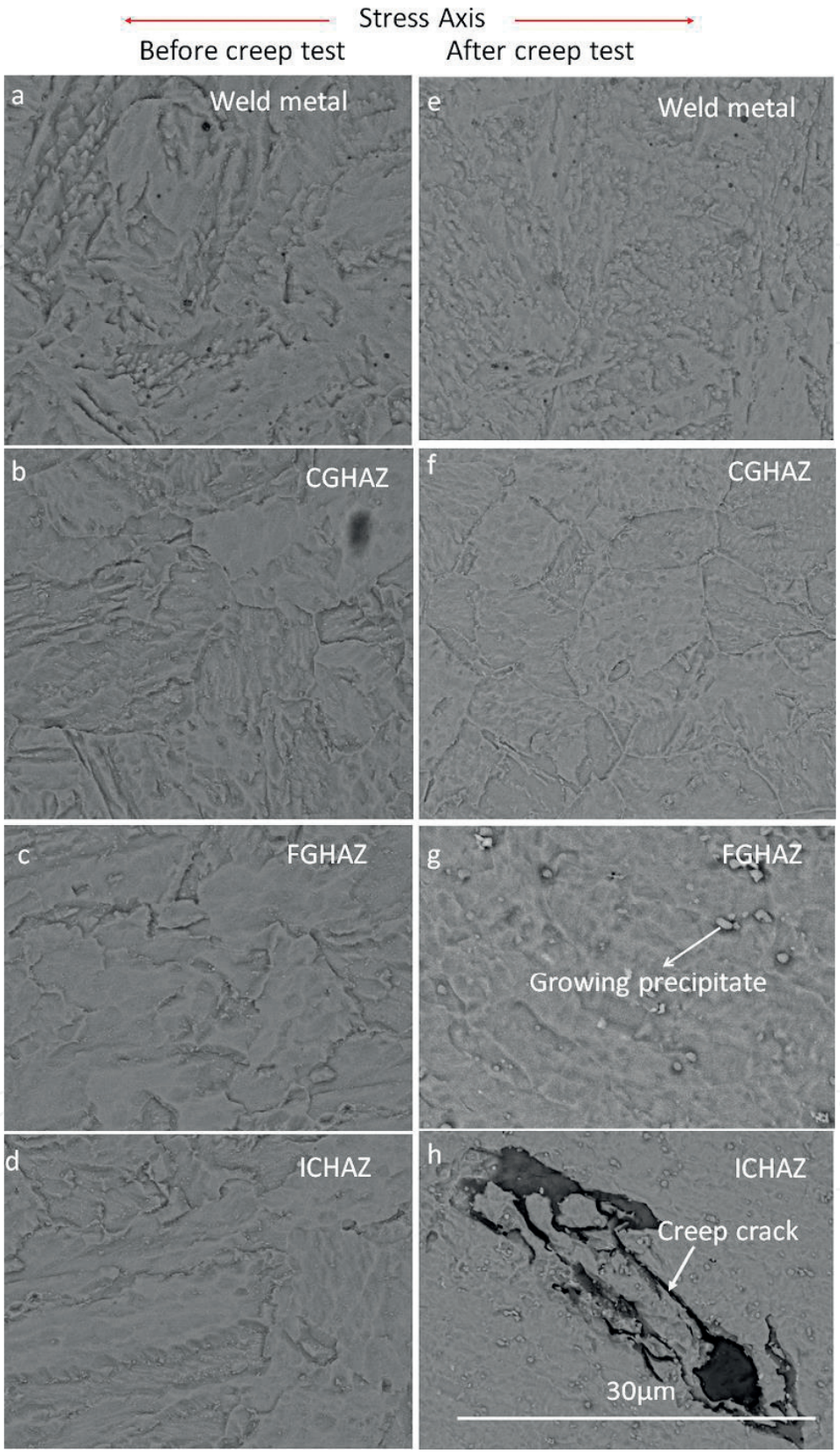

Figure 6. SEM-BSE micrographs showing the microstructures at different locations across the weldments: (a–d) before creep testing and (e–h) after creep testing (creep exposure at 650°C/50 MPa and rupture time is 3772 h) [60].

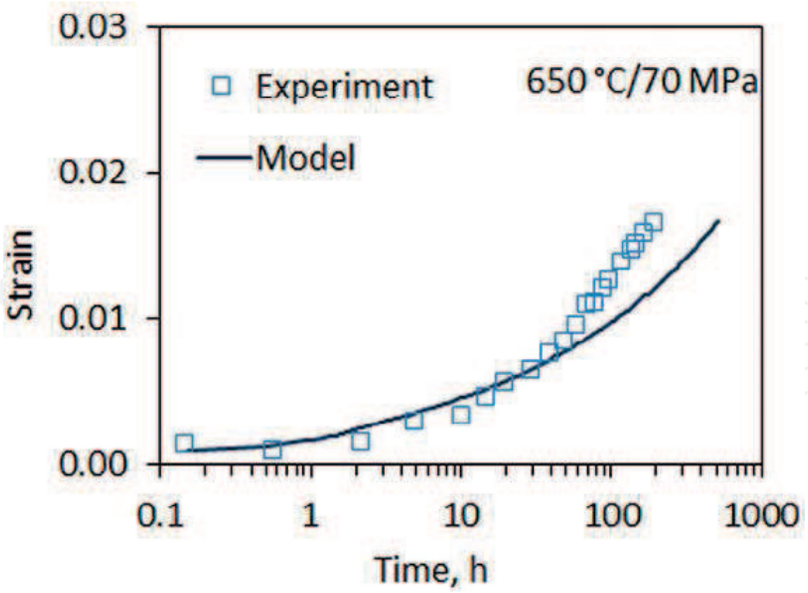

Figure 7. Comparison of creep strain time curves between experiment and FEA for composite structure at 650°C/70 MPa [60].

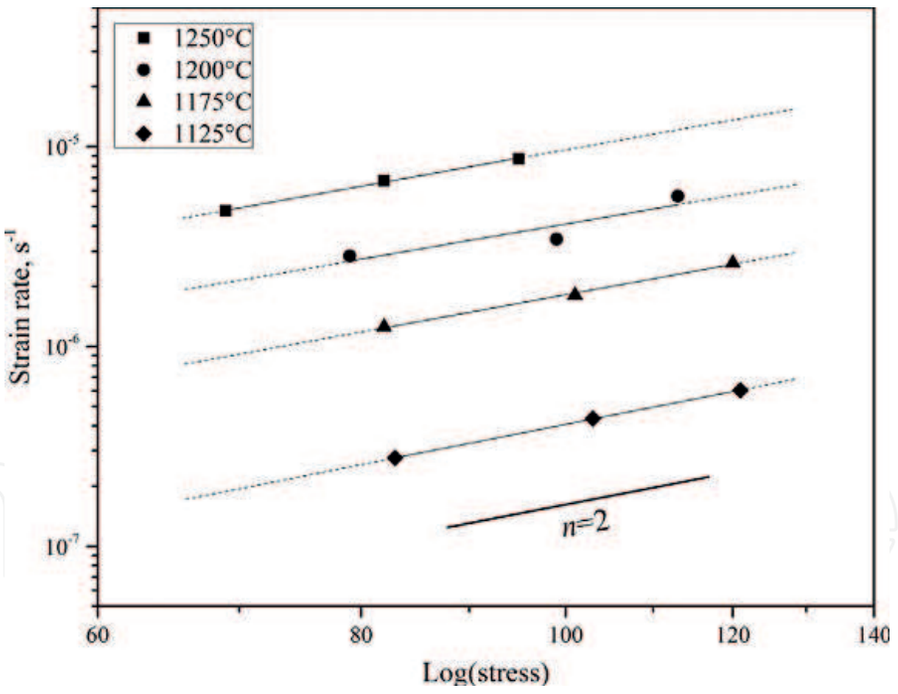

Figure 8. Creep rates of alumina as a function of true stress [63].

Copper gives creep strain versus time curves at 75°C, which look very similar to those recorded at much higher temperatures. Thus, an extended secondary stage where the strain rate is constant is observed. Considering the high creep exponent that can be up to 75, one would expect a creep curve with rapidly increasing strain rate but that is not found. The difference of creep of pure metals at high temperatures is so large that we can talk about

an entirely new material class with respect to creep. To explain the observations, a recently developed dislocation model (Sandstrom, 2017) for cell structures is used.

A new creep model was presented where a back stress based on the dislocations in the cell walls is introduced. Unbalanced sets of dislocations without matching dislocations of opposite signs are formed in the cell walls. Since the unbalanced content is not exposed to static recovery, it forms a stable back stress. It was shown that the computed back stress can fully explain the observations and reproduce both creep curves and results for slow strain rate tensile tests [64]. Also, the creep behavior of alumina has been investigated [65–77]. There are numerous instances of the structural application of GFRP in the construction of buildings and bridges [78, 79]. Exceptional reviews of the widespread studies on the topic may be found in some important references [80–82]. Also, some studies were done regarding the proposition of quantum mechanical tunneling of dislocations at very low temperature [83–88].

Till now, numerous constitutive models have been presented to address viscoplastic, plasticity and the creep behaviors of materials [89–107]. Also, the time-dependent creep deformation of a metallic component under applied stress and temperature was studied by many researchers [92, 99, 104, 105].

Creep rupture and failure of the creeping metals are dedicated to the basic explanation of the creep which happens extensively in high-temperature deformation of the creeping metals. Particular concentration and attention are paid to the analysis of long-term strength, which characterizes the stress at which the creeping metal does not fail after a predetermined time. Lokoshchenko [106] details experimental and analytical results determined by Soviet and Russian scientists who are absent in presently accessible publications and demonstrates theoretical models and methods to attain long-term strength in metals [106].

As another interesting book, the third edition of fundamentals of creep in metals and alloys [105] stays generally up to date for the creeping metals, there are a wide range of improvements and updates that are either pleasing, or necessary, to make sure that the book continues to meet the needs of the investigators in the general area of steady state creep plasticity (time-dependent plasticity, viscoplastic and viscoelastic). As well, updating the areas presently covered in the second edition with new advances, the third edition will broaden its scope beyond metals and alloys to include ceramics, covalent solids, minerals and polymers, hence addressing the fundamentals of creep in all fundamental classes of the creeping materials [105].

6. Solved problems

Problem 6.1. Determine the viscosity of the creeping fibrous composites semi-theoretically.

Solution:
A semi-analytical formulation is presented for obtaining the viscosity of solids (such as metals) using the steady state creep model of the short fiber composites. For achieving this aim, fluid mechanics theory is used for determining the viscosity. Sometimes, obtaining the viscosity is

experimentally difficult and intricate. Therefore, the present model may be beneficial to obtain the viscosity of metals (see **Figure 9**).

Figure 9 graphically shows a simple simulation and analogy between the steady state creep behavior of the short fiber composite and viscosity of the viscous fluid. The shear stress is generally defined by the following equation in the creeping solids at any given arbitrary $r = r_0$ and $z = z_0$ mathematically,

$$\tau_{rz}^{matrix} = a_0 \ln z + a_1 \tag{10}$$

where the constants "a_0" and "a_1" are introduced in Eqs. (17a, b). On the other hand, the shear stress in the fluids is given by:

$$\tau_{rz}^{fluid} = \mu \dot{\gamma}_{rz}^{fluid} \tag{11}$$

where the parameters "μ" and "$\dot{\gamma}$" are the viscosity and shear strain rate, respectively. The shear strain rate "$\dot{\gamma}$" is defined as follows:

$$\dot{\gamma}_{rz} = \frac{\partial \dot{w}}{\partial r} + \frac{\partial \dot{u}}{\partial z} \tag{12}$$

Now, the average shear stress at the interface is obtained for determining the viscosity "μ" as follows:

$$\tau_{rz}^{matrix}\Big|_{average}^{r=a} = \frac{1}{l}\int_0^l (a_0 \ln z + a_1)\, dz \tag{13}$$

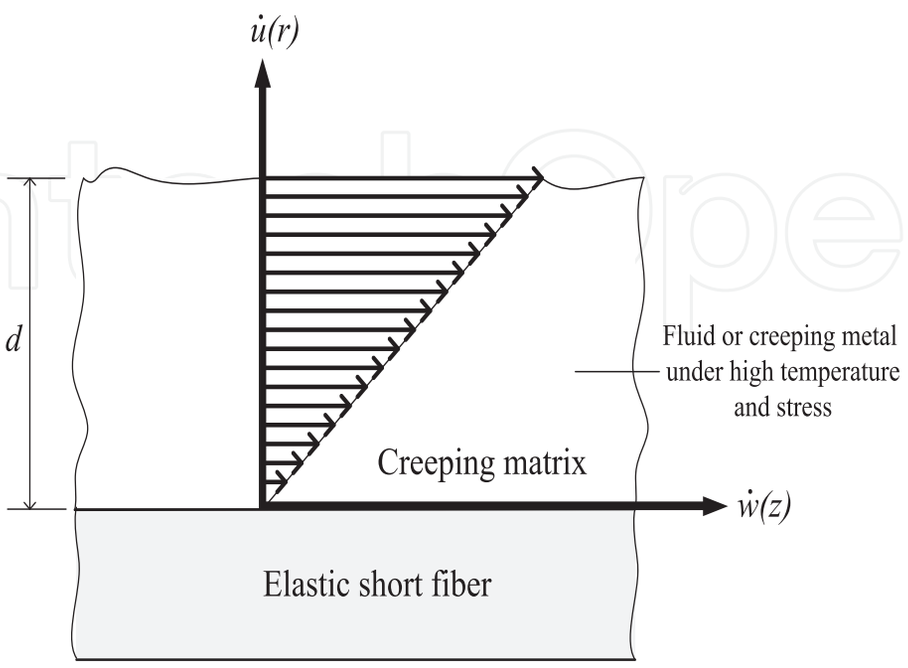

Figure 9. Simulation between creeping composite and viscous fluid.

Thus, the viscosity "μ" is determined by the combination of Eqs. (10)–(13), which yields

$$\mu = \frac{\tau_{rz}^{matrix}\Big|_{average}^{r=a}}{\dot{\gamma}_{rz}^{matrix}} \tag{14}$$

To summarize the calculations, previously published research results [13] are used for obtaining the viscosity "μ" (Eq. (14)). Therefore, the viscosity of the creeping matrix in the short fiber composite is determined using fluid mechanics and creep theories. Finally, the viscosity of the metals at the mentioned temperatures "μ" is semi-analytically obtained by the following relation:

$$\left[\tau_{matrix}\right]_{creep\ of\ composite}^{obtained\ \ using\ available\ results\ [13,22-24]} = \left[\tau_{viscous\ fluid}\right]_{fluid}^{viscosity"\mu"is\ unknown} = \mu\dot{\gamma}_{fluid} = \mu\left(\frac{\partial\dot{w}}{\partial r} + \frac{\partial\dot{u}}{\partial z}\right) \tag{15}$$

where $\dot{u}$ (radial displacement rate) and $\dot{w}$ (axial displacement rate) are obtained using the obtained results presented in [13, 22–24]. Moreover, the creeping shear stress "τ_{matrix}" is presented in Eqs. (17a, b). For the fibrous composite employed here "*SiC/Al6061,*" the volume fraction of the fibers is approximately *15%* and the fibers have an aspect ratio of *7.4* and $k = 0.76$, which are according to the Ref. [36]. In addition, the second-stage creep constants of the creeping matrix material, A and B, in Eq. (16) at $300^{\circ}C$ are considered as $A = exp.(-24.7)$ and $B = 6.47$, given by Morimoto et al. [36].

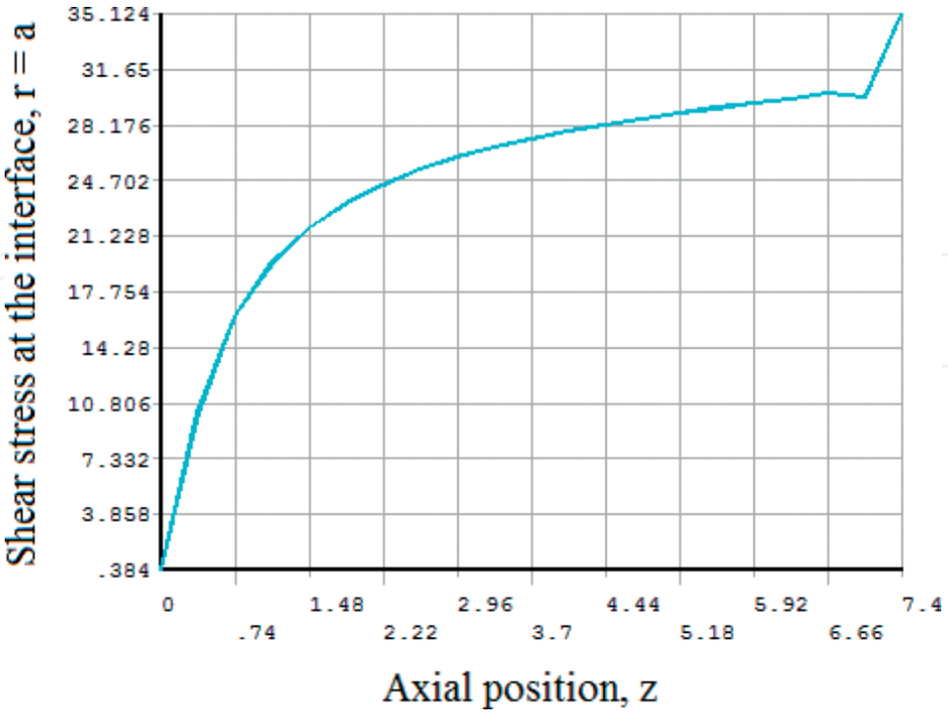

Figure 10. Shear stress behavior in the creeping metal matrix composite in the steady state creep (at interface, $r = a$, with the assumption of $a = 1$).

$$\dot{\varepsilon}_e = Aexp\left(\frac{\sigma_e}{B}\right) \tag{16}$$

where σ_e and $\dot{\varepsilon}_e$ are the equivalent stress and equivalent strain rate of the creeping matrix, respectively. A quantitative example is presented in this section. The interfacial shear stress is in the following form mathematically:

$$\tau_i = \tau_{rz}^{fluid}|_{r=a} = \mu\dot{\gamma}_{rz}^{fluid}|_{r=a} \tag{17}$$

$$\tau_i = 3.75 \ln\left(\frac{z}{l}\right) + 27.2 \tag{18}$$

Shear stress presented in Eqs. (17a, b) is graphically shown in **Figure 10**.

The average shear stress, τ_{rz}^{matrix} (at interface, $r = a$), is obtained by Eq. (13). Also, the shear strain rate, $\dot{\gamma}_{rz}^{matrix}$, is determined by Eq. (12). By a simple calculation, the viscosity,μ, for the mentioned metal *Al6061* under the mentioned conditions is approximately equal to $4.8 \times 10^{15}\lambda$ Pa.s, in which the parameter of "λ" is a positive and small number. Also, FEM nodal solution of the

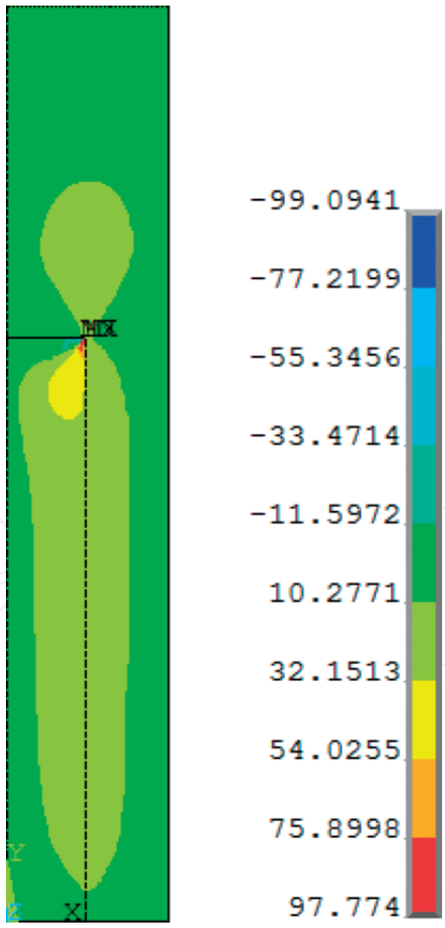

Figure 11. FEM nodal solution of the unit cell for predicting the shear stress behavior (the distribution of the shear stresses in the unit cell) [x = r(radial), y = z(axial) and z = θ(circumferential)].

unit cell for predicting the shear stress behavior is shown in **Figure 11** for better understanding the shear stress behavior in the steady state creep of the short fiber composites. **Figures 10** and **11** are presented with an assumption of $a = 1$.

For comparison purpose, the viscosity of pitch at $298\ K$ is equal to 2.3×10^8 Pa.s [34]. The results of the present method for obtaining the viscosity have a good agreement with the other available research results. The value of the mentioned viscosity is logical in comparison with the available results. In this problem, a novel approach was introduced to obtain the viscosity of the metals using the creeping property of the composites.

In addition, the behavior of the creeping metals under applied stress and temperature was simulated with the viscous fluids. The present method is useful and applicable for obtaining the viscosity, because the expensive and time-consuming experimental methods have many difficulties in determining the viscosity of the metals at high temperatures. Also, sometimes obtaining the viscosity of the metals at some temperatures is very intricate. Finally, this method can be used for obtaining the viscosity of the metals under different conditions using the steady state creeping property of the composites [50].

Problem 6.2. The Cauchy stress tensor components at one point of a creeping material (second-stage creep) considering Newtonian fluid, in which the bulk viscosity coefficient is zero, are given by:

$$\sigma_{ij} = \begin{bmatrix} -1 & 1 & -1 \\ 1 & -5 & 3 \\ -1 & 3 & -3 \end{bmatrix} Pa \tag{19}$$

Obtain the viscous stress tensor components in a creeping material (such as creeping matrix in composites).

Solution:

If the bulk viscosity coefficient is zero, Stokes' condition, we will have, $p = p_{ave} = p_0$, and moreover, we may determine

$$\sigma_{ij} = -p\delta_{ij} + \tau_{ij} \tag{20}$$

Also, have

$$\kappa = \lambda + \frac{2}{3}\mu = 0 \tag{21}$$

It yields

$$\sigma_{ii} = -3p \tag{22}$$

$$p = -\frac{\sigma_{ii}}{3} = -\frac{(-1-5-3)}{3} = 3 \tag{23}$$

Therefore, we have

$$\tau_{ij} = \sigma_{ij} + p\delta_{ij} = \begin{bmatrix} -1 & 1 & -1 \\ 1 & -5 & 3 \\ -1 & 3 & -3 \end{bmatrix} + \begin{bmatrix} 3 & 0 & 0 \\ 0 & 3 & 0 \\ 0 & 0 & 3 \end{bmatrix} = \begin{bmatrix} 2 & 1 & -1 \\ 1 & -2 & 3 \\ -1 & 3 & 0 \end{bmatrix} Pa \tag{24}$$

Problem 6.3. Assume that the Cauchy stress tensor components at the point P of a creeping material (steady state creep) are given by the following form:

$$\sigma_{ij} = \begin{bmatrix} 1 & 6 & 7 \\ 6 & 7 & 9 \\ 7 & 9 & 4 \end{bmatrix} GPa \tag{25}$$

a) Determine the hydrostatic stress (mean stress).

b) Obtain the deviatoric and spherical part of the stress tensor of "σ".

Solution:

a) The hydrostatic stress (mean stress) is given by the following equation:

$$\sigma_m = \sigma_{Hyd} = \frac{\sigma_{ii}}{3} = \frac{1+7+4}{3} = 4 \tag{26}$$

b) The spherical part of stress tensor "σ" is given by the following equation:

$$\sigma_{ij}^{sph} = \frac{I_\sigma}{3}\delta_{ij} = \sigma_{Hyd}\delta_{ij} = \begin{bmatrix} \sigma_{Hyd} & 0 & 0 \\ 0 & \sigma_{Hyd} & 0 \\ 0 & 0 & \sigma_{Hyd} \end{bmatrix} = \begin{bmatrix} 4 & 0 & 0 \\ 0 & 4 & 0 \\ 0 & 0 & 4 \end{bmatrix} \tag{27}$$

And the Deviatoric part becomes as follows:

$$\sigma_{ij} = \sigma_{ij}^{sph} + \sigma_{ij}^{dev} \tag{28}$$

Therefore,

$$\sigma_{ij}^{dev} = \sigma_{ij} - \sigma_{ij}^{sph} \tag{29}$$

Finally,

$$\sigma_{ij}^{dev} = \begin{bmatrix} -3 & 6 & 7 \\ 6 & 3 & 9 \\ 7 & 9 & 0 \end{bmatrix} GPa \tag{30}$$

Problem 6.4. The below second-stage creep data have been taken on an aluminum alloy at 400°**C** and a constant stress of 25 MPa (see **Table 1**). Draw the following data as strain versus time, and after that obtain the steady state or minimum creep rate generally and approximately. Comment: The preliminary and immediate strain is not included (Based on University of California San Diego's (UCSD) exams).

Solution:

These creep data are plotted as shown in **Figure 12**.

Time (min)	Strain	Time (min)	Strain
0	0.000	16	0.135
2	0.025	18	0.153
4	0.043	20	0.172
6	0.065	22	0.193
8	0.078	24	0.218
10	0.092	26	0.255
12	0.109	28	0.307
14	0.120	30	0.368

Table 1. Aluminum alloy at 400°C and a constant stress of 25 *MPa*.

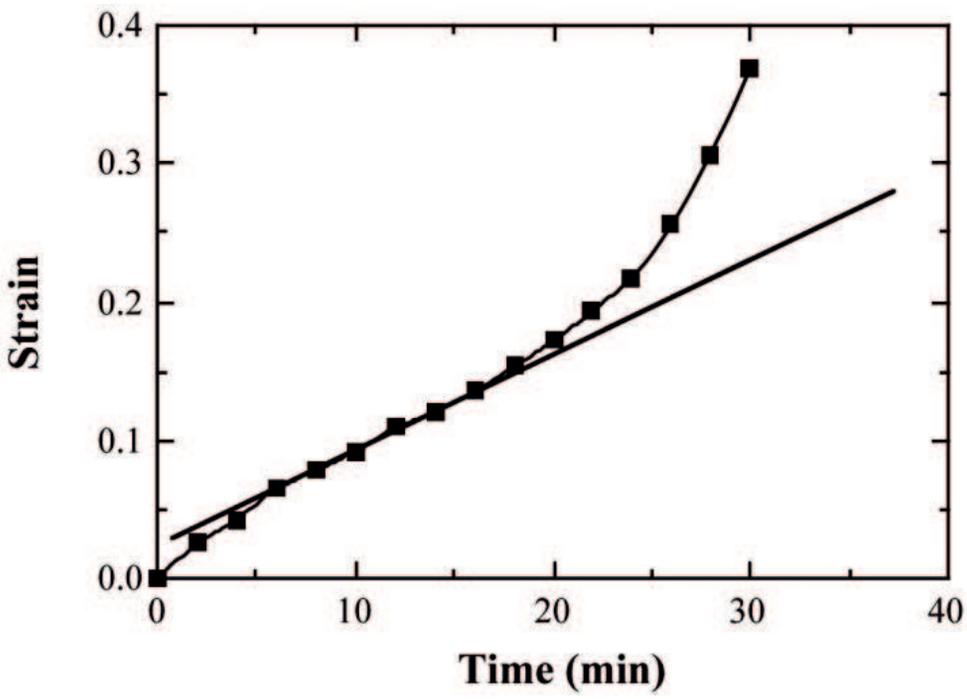

Figure 12. Plotted creep data.

The steady state creep rate ($\Delta\varepsilon/\Delta t$) is the slope of the linear region. The straight line has been superimposed on the curve.

Problem 6.5. Steady state creep rate data for nickel at 1000°C (1273 K) are given in **Table 2**:

If it is known that the activation energy for creep is 272,000 J/mol, compute the steady state creep rate at a temperature of 850°C (1123 K) and a stress level of 25 MPa (3625 psi) (based on University of California San Diego's (UCSD) exams).

Solution:

Taking natural logarithms of both sides of the following equation yield,

$$\dot{\varepsilon}_s = K\sigma^n \exp\left(-\frac{Q_c}{RT}\right) \tag{31}$$

$$ln(\dot{\varepsilon}_s) = \ln(K) + n\ln(\sigma) - \frac{Q_c}{RT} \tag{32}$$

With the given data, there are two unknowns in this equation (namely K and n). Using the data provided in the problem statement, we can set up two independent equations as follows:

$$ln\left(1 \times 10^{-4}\right) = \ln(K) + n\ln(15) - \frac{272000}{8.31 \times 1273} \tag{33}$$

$$ln\left(1 \times 10^{-6}\right) = \ln(K) + n\ln(4.5) - \frac{272000}{8.31 \times 1273} \tag{34}$$

Therefore, we have

n = 3.825, K = 466 1/s.

Thus, it is now possible to solve at 25 *MPa* and *1123 K* using the mentioned equation.

$$\dot{\varepsilon}_s = K\sigma^n \exp\left(-\frac{Q_c}{RT}\right) = 466 \times 25^{3.825} \exp\left(-\frac{272000}{8.31 \times 1273}\right) = 2.28 \times 10^{-5}\ s^{-1} \tag{35}$$

$\dot{\varepsilon}_s\left(s^{-1}\right)$	**σ[MPa (psi)]**
10^{-4}	15 (2175)
10^{-6}	4.5 (650)

Table 2. Data of nickel at 1000°C (1273 K).

Author details

Vahid Monfared

Address all correspondence to: vahid_monfared_57@yahoo.com;
vahid_monfared@alum.sharif.edu

Department of Mechanical Engineering, Zanjan Branch, Islamic Azad University, Zanjan, Iran

References

[1] Cox HL. The elasticity and strength of paper and other fibrous materials. British Journal of Applied Physics. 1952;**3**:72-79

[2] Mileiko ST. Steady state creep of a composite with short fibres. Journal of Materials Science. 1970;**5**:254-261

[3] McLean D. Viscous flow of aligned composites. Journal of Materials Science. 1972;**7**: 98-104

[4] Fukuda H, Chou TW. An advanced shear-lag model applicable to discontinuous fiber composites. Journal of Composite Materials. 1981;**15**(**1**):79-91

[5] McLean M. Creep deformation of metal matrix composites. Composites Science and Technology. 1985;**23**:37-52

[6] Lee YS, Batt TJ, Liaw PK. Stress analysis of a composite material with short elastic fibre in power law creep matrix. International Journal of Mechanical Sciences. 1990;**32**(10): 801-815

[7] Pachalis JR, Kim J, Chou TW. Modeling of creep of aligned short-fiber reinforced ceramic composites. Composites Science and Technology. 1990;**37**:329-346

[8] Wang YR, Chou TW. Analytical modeling of creep of short fiber reinforced ceramic matrix composite. Journal of Composite Materials. 1992;**26**(9):1269-1286

[9] Durodola JF, Ruiz C, Derby B. Uniaxial creep of long fibre reinforced metal matrix composites. Composites Engineering. 1994;**4**(12):1241-1255

[10] Zhang J. Modeling of the influence of fibers on creep of fiber reinforced cementitious composite. Composites Science and Technology. 2003;**63**(13):1877-1884

[11] Gao XL, Li K. A shear-lag for carbon nanotube-reinforced polymer composites. International Journal of Solids and Structures. 2005;**42**:1649-1667

[12] Mondali M, Abedian A, Ghavami A. A new analytical shear-lag based model for prediction of the steady state creep deformations of some short fiber composites. Materials & Design. 2009;**30**:1075-1084

[13] Mondali M, Monfared V, Abedian A. Non-linear creep modeling of short fiber composites using Hermite polynomials, hyperbolic trigonometric functions and power series. Comptes rendus Mecanique. 2013;**341**(7):592-604

[14] Weng GJ, Sun CT. Effects of fiber length on the elastic moduli of randomly oriented chopped-fiber composites. In: Tsai SW, editor. ASTM-STP-674Composite Materials: Testing and Design. 1979. pp. 149-162

[15] Hsueh CH. A modified analysis for stress transfer in fiber-reinforced composites with bonded fiber ends. Journal of Materials Science. 1995;**30**:219-224

[16] Nayfeh AH, Abdelrahman WG. Micromechanical modeling of load transfer in fibrous composites. Mechanics of Materials. 1998;**30**:307-324

[17] Jiang Z, Liu X, Li G, Lian J. A new analytical model for three-dimensional elastic stress field distribution in short fibre composite. Materials Science and Engineering. 2004;**A366**:381-396

[18] Abedian A, Mondali M, Pahlavanpour M. Basic modifications in 3D micromechanical modeling of short fiber composites with bonded and debonded fiber end. Computational Materials Science. 2007;**40**:421-433

[19] Schjødt-Thomsen J, Pyrz R. Non-linear creep modelling of single-fibre model composites. Composites Science and Technology. 2000;**60**(9):1791-1800

[20] Kumar S, Singh RN. The creep response of uni-directional fiber-reinforced ceramic composites: A theoretical study. Composites Science and Technology. 2001;**61**(4):461-473

[21] Ohno N, Ando T, Miyake T, Biwa S. A variational method for unidirectional fiber-reinforced composites with matrix creep. International Journal of Solids and Structures. 2002;**39**(1):159-174

[22] Monfared V, Mondali M, Abedian A. Steady state creep behavior of short fiber composites by mapping, logarithmic functions (MF) and dimensionless parameter (DP) techniques. Archives of Civil and Mechanical Engineering. 2012;**12**(4):455-463

[23] Monfared V, Mondali M, Abedian A. Steady state creep analysis of polymer matrix composites using complex variable method. Proceedings of the Institution of Mechanical Engineers Part C-Journal of Mechanical Engineering Science. 2013;**227**(10):2182-2194

[24] Monfared V, Mondali M, Abedian A. Novel mathematical approaches for analyzing time dependent creep deformations in reinforced metals. Journal of Mechanical Science and Technology. 2013;**27**(11):3277-3285

[25] Dragon TL, Nix WD. Geometric factors affecting the internal stress distribution and high temperature creep rate of discontinuous fiber reinforced metals. Acta Metallurgica et Materialia. 1990;**38**(10):1941-1953

[26] Povirk GL, Needleman A, Nutt SR. An analysis of residual stress formation in whisker-reinforced al/SiC composites. Materials Science and Engineering. 1990;**A125**(2):129-140

[27] Levy A, Papazian JM. Elastoplastic finite element analysis of short-fiber-reinforced SiC/al composites: Effects of thermal treatment. Acta Metallurgica et Materialia. 1991;**39**(10): 2255-2266

[28] Park YH, Holmes JW. Finite element modeling of creep deformation in fibre-reinforced ceramic composites. Journal of Materials Science. 1992;**27**(23):6341-6351

[29] Davis LC, Allison JE. Micromechanics effects in creep of metal-matrix composites. Metallurgical and Materials Transactions A. 1995;**26**(12):3081-3089

[30] Zhu-feng Y. Statistic modeling of the creep behavior of metal matrix composites based on finite element analysis. Applied Mathematics and Mechanics. 2002;**23**(4):421-434

[31] Mondali M, Abedian A, Adibnazari S. FEM study of the second stage creep behavior of Al6061/SiC metal matrix composite. Computational Materials Science. 2005;**34**:140-150

[32] Ghavami A, Abedian A, Mondali M. Finite difference solution of steady state creep deformations in a short fiber composite in presence of fiber/matrix debonding. Materials & Design. 2010;**31**:2616-2624

[33] Monfared V, Mondali M. Semi-analytically presenting the creep strain rate and quasi shear-lag model as well as FEM prediction of creep Debonding in short fiber composites. Materials & Design. 2014;**54**:368-374

[34] Edgeworth R, Dalton BJ, Parnell T. The pitch drop experiment. European Journal of Physics. 1984;**5**:198-200

[35] Nieh TG. Creep rupture of a silicon-carbide reinforced aluminum composite. Metallurgical and Materials Transactions A. 1984;**15**:139-146

[36] Morimoto T, Yamaoka T, Lilholt H, Taya M. Second stage creep of silicon carbide whisker/6061 aluminum composite at 573K. Journal of Engineering Materials and Technology. 1988;**110**:70-76

[37] Zhu SJ, YX L, Wang ZG, Bi J. Creep behavior of TiC-particulate-reinforced Ti alloy composite. Materials Letters. 1992;**13**(4-5):199-203

[38] Čadek J, Oikawa H, Šustek V. Threshold creep behaviour of discontinuous aluminium and aluminium alloy matrix composites: An overview. Materials Science and Engineering A. 1995;**190**(1-2):9-23

[39] Matsuda N, Akaike J, Hongo K, Matsuura K. The effect of second phase on the creep deformation of 6061Al matrix composites. Materials Science and Engineering A. 1997; **234-236**:751-754

[40] Cseh G, Bär J, Gudladt HJ, Lendvai J, Juhász A. Indentation creep in a short fibre-reinforced metal matrix composite. Materials Science and Engineering A. 1999;**272**(1):145-151

[41] Wang M, Zhao Y, Zhou L, Zhang D. Study on creep behavior of Ti–V–Cr burn resistant alloys. Materials Letters. 2004;**58**(26):3248-3252

[42] Kouadri-Boudjelthia A, Imad A, Bouabdallah A, Elmeguenni M. Analysis of the effect of temperature on the creep parameters of composite material. Materials & Design. 2009;**30**(5): 1569-1574

[43] Mahmudi R, Geranmayeh AR, Khanbareh H, Jahangiri N. Indentation creep of lead-free Sn–9Zn and Sn–8Zn–3Bi solder alloys. Materials & Design. 2009;**30**(3):574-580

[44] Olbricht J, Yawny A, Young ML, Eggeler G. Mechanical and microstructural observations during compression creep of a short fiber reinforced AlMg metal matrix composite. Materials Science and Engineering A. 2009;**510-511**:407-412

[45] Morscher GN, John R, Zawada L, Brewer D, Ojard G, Calomino A. Creep in vacuum of woven Sylramic-iBN melt-infiltrated composites. Composites Science and Technology. 2011;**71**(1):52-59

[46] Soubielle S, Diologent F, Salvo L, Mortensen MA. Creep of replicated microcellular aluminium. Acta Materialia. 2011;**59**(2):440-450

[47] Tang XG, Hou M, Zou J, Truss R, Zhu Z. The creep behaviour of poly(vinylidene fluoride)/"bud-branched" nanotubes nanocomposites. Composites Science and Technology. 2012;**72**(14):1656-1664

[48] Li LT, Lin YC, Zhou HM, Jiang YQ. Modeling the high-temperature creep behaviors of 7075 and 2124 aluminum alloys by continuum damage mechanics model. Computational Materials Science. 2013;**73**:72-78

[49] Tang LC, Wang X, Gong LX, Peng K, Zhao L, Chen Q, LB W, Jiang JX, Lai GQ. Creep and recovery of polystyrene composites filled with graphene additives. Composites Science and Technology. 2014;**91**:63-70

[50] Monfared V. Predicting the viscosity of solids using steady-state creep behavior of the fibrous composites semi-theoretically. Results in Physics. 2017;**7**:1433-1436

[51] Monfared V. Neural network based simulation of micro creeping fibrous composites SIC/AL6061 for plastic behavior. Journal of Theoretical and Applied Mechanics, Sofia. 2017;**47**(1):36-48

[52] Monfared V. Role of high order functions in analysis of the creep behavior of a short fiber composite "silicon carbide/aluminum 6061". Silicon. 2017;**9**(3):339-345

[53] Ma X, Li F, Zhao C, Zhu G, Li W, Sun Z, Yuan Z. Indenter load effects on creep deformation behavior for Ti-10V-2Fe-3Al alloy at room temperature. Journal of Alloys and Compounds. 2017;**709**:322-328

[54] Wei J, Malzbender J. Steady state creep of Ni-8YSZ substrates for application in solid oxide fuel and electrolysis cells. Journal of Power Sources. 2017;**360**:1-10

[55] Zhang Y, Jing H, Xu L, Zhao L, Han Y, Liang J. Microstructure and texture study on an advanced heat-resistant alloy during creep. Materials Characterization. 2017;**130**:156-172

[56] Coakley J, Ma D, Frost M, Dye D, Seidman DN, Dunand DC, Stone HJ. Lattice strain evolution and load partitioning during creep of a Ni-based superalloy single crystal with rafted γ′ microstructure. Acta Materialia. 2017;**135**:77-87

[57] Reddy KV, Md M, Pal S. Mechanistic study of bending creep behaviour of bicrystal nanobeam. Computational Materials Science. 2017;**136**:36-43

[58] Pandey C, Mahapatra MM, Kumar P, Saini N. Effect of creep phenomena on room-temperature tensile properties of cast & forged P91 steel. Engineering Failure Analysis. 2017;**79**:385-396

[59] Jiang X, Zhang Y, Yi D, Wang H, Deng X, Wang B. Low-temperature creep behavior and microstructural evolution of 8030 aluminum cables. Materials Characterization. 2017; **130**:181-187

[60] Baral J, Swaminathan J, Chakrabarti D, Ghosh RN. Effect of welding on creep damage evolution in P91B steel. Journal of Nuclear Materials. 2017;**490**:333-343

[61] Lin C, Tian Q, Chen K, He G, Zhang J, Liu S, Almásy L. Polymer bonded explosives with highly tunable creep resistance based on segmented polyurethane copolymers with different hard segment contents. Composites Science and Technology. 2017;**146**:10-19

[62] Ni T, Dong J. Creep behaviors and mechanisms of Inconel718 and Allvac718plus. Materials Science and Engineering A. 2017;**700**:406-415

[63] Ratzker B, Sokol M, Kalabukhov S, Frage N. Using a spark plasma sintering apparatus as a tool in a compressive creep study of fine-grained alumina. Ceramics International. 2017;**43**(12):9369-9376

[64] Sandström R. Formation of a dislocation back stress during creep of copper at low temperatures. Materials Science and Engineering A. 2017;**700**:622-630

[65] Folweiler RC. Creep behavior of pore free polycrystalline aluminum oxide. Journal of Applied Physics. 1961;**32**(5):773-778

[66] Arshaw SIW, Norton FH. Deformation behavior of polycrystalline aluminum. Journal of the American Ceramic Society. 1962;**45**(10):479-486

[67] Coble RL, Guerard YH. Creep of polycrystalline aluminum oxide. Journal of the American Ceramic Society. 1963;**46**(7):353-354

[68] Paladino AE, Coble RL. Effect of grain boundaries on diffusion-controlled processes in aluminum oxide. Journal of the American Ceramic Society. 1963;**46**(3):133-136

[69] Cannon RM, Rhodes WH, Heuer AH. Plastic deformation of fine-grained alumina (Al2O3):I, interface-controlled diffusional creep. Journal of the American Ceramic Society. 1980;**63**(1–2):46-53

[70] Heuer AH, Tighe NJ, Cannon RM. Plastic deformation of fine-grained alumina (Al2O3): II, basal slip and non accommodated grain-boundary sliding. Journal of the American Ceramic Society. 1980;**63**(1-2):53-58,1980

[71] Xue LA, Chen I. Deformation and grain growth of low-temperature-sinteredhigh- purity alumina. Journal of the American Ceramic Society. 1990;**73**(11):3518-3521

[72] Wang J, Raj R. Interface effects in super plastic deformation of alumina containing zirconia, titania or hafnia as a second phase. Acta Metallurgica et Materialia. 1991;**39**(11):2909-2019

[73] Nutt SR, Lipetzky P. Creep deformation of whisker-reinforced alumina. Materials Science and Engineering A. 1993;**166**(1):199-209

[74] Flacher O, Blandin JJ, Plucknett KP. Effects of zirconia additions on the super plasticity of alumina-zirconia composites. Materials Science and Engineering A. 1996;**221**:102-112

[75] Chevalier J, Olagnon C, Fantozzi G, Gros H. Creep behavior of alumina, zirconia and zirconia-toughened alumina. Journal of the European Ceramic Society. 1997;**7**(6):859-864

[76] Ruano OA, Wadsworth J, Sherby OD. Deformation of fine-grained alumina by grain boundary sliding accommodated by slip. Acta Materialia. 2003;**51**(12):3617-3634

[77] Bernard-Granger G, Guizard C, Duclos R. Compressive creep behavior in air of a slightly porousas-sintered polycrystalline α-alumina material. Journal of Materials Science. 2007;**42**(8):2807-2819

[78] Scott DW, Lai JS, Zureick A-H. Creep behavior of FRP composites: Are view of technical literature. Journal of Reinforced Plastics and Composites. 1995;**14**:588-617

[79] Keller T. Use of fibre reinforced polymers in bridge construction. In: Structural Engineering Documents. Vol. 7. IABSE, Zurich, Switzerland: International Association for Bridge and Structural Engineering; 2003

[80] Lupinc V. In: Bressers J, editor. Creep and Fatigue in High Temperature Alloys. London: Applied Science Publishers; 1981. pp. 7-40

[81] Lagneborg R. In: Bressers J, editor. Creep and Fatigue in High Temperature Alloys. London: Applied Science Publishers; 1981. pp. 41-71

[82] Wilshire B, Burt H. Damage evolution during creep of steels. International Journal of Pressure Vessels and Piping. 2008;**85**:47-54

[83] Mott NF. Creep in metal crystals at very low temperatures. Philosophical Magazine. 1956;**1**(6):568-572

[84] Glen JW. The creep of cadmium crystals at liquid helium temperatures. Philosophical Magazine. 1956;**1**(5):400-408

[85] Arko AC, Weertman J. Creep deformation of Cd and Hg at liquid helium temperatures. Acta Metallurgica. 1969;**17**:687-699

[86] Tesh JR, Whitworth RW. Plastic deformation and creep if sodium chloride crystals at liquid helium temperatures. Physica Status Solidi. 1970;**39**:627-633

[87] Osetskii AI, Soldatov VP, Startsev VI, Natsik VD. Temperature dependence and activation parameters of creep in Zn in the temperature range 1.5 to 80 K. Physica Status Solidi A. 1974;**22**:739-748

[88] Startsev VI, Soldatov VP, Natsik VD, Abraimov VV. Role of quantum mechanisms and thermal heating in low-temperature creep of metals. Physica Status Solidi A. 1980;**59**:377-388

[89] Lubahn JD, Felgar RP. Plasticity and Creep of Metals. Wiley series on the science and technology of materials. Canada: Wiley; 1961

[90] Garofalo F. Fundamentals of Creep and Creep-Rupture in Metals, MacMillan Series in Materials. United States: MacMillan and Co; 1965

[91] Wilcox BA. Steady-State Creep of Dispersion-Strengthened Metals. United States: NASA; 1966

[92] Rabotnov YN. Creep Problems in Structural Memberse. NewYork, NY: American Elsevier Publishing Company. Inc.; 1969

[93] Greenfield P. Creep of Metals at High Temperature (Mechanics Engineering Monograph). Great Britain: Mills & Boon; 1972

[94] Frost HJ, Ashby MF. Deformation-Mechanism Maps: The Plasticity and Creep of Metals and Ceramics. United States (University of Michigan): Pergamon Press; 1982

[95] Boyle JT, Spence J. Stress Analysis for Creep. 1st ed. Southampton: Butterworth, UK: Butterworth-Heinemann; 1983

[96] Evans RW, Wilshire B. Creep of Metals and Alloys (Predictive and Quantitative Metallurgy Series). London (Institute of Metals): CRC Press; 1985

[97] Zyczkowski M. Creep in structures: 4th IUTAM Symposium. Cracow, Poland. 1990: 10–14 (IUTAM Symposia), Springer; Softcover reprint of the original 1st ed. 1991 edition

[98] Khan AS, Huang S. Continuum Theory of Plasticity. 1st ed. New York: John Wiley & Sons; 1995

[99] Nabarro FRN, Villiers HL de. The Physics of Creep.1995. Taylor & FrancisInc, Bristol, PA

[100] Mishra RS, Earthman JC. Creep Deformation: Fundamentals and Applications. Pittsburgh, PA, United States: Tms; 2002

[101] Betten J. Creep Mechanics. 2nd ed. Germany: Springer; 2005

[102] Abe F, Kern TU. Creep-Resistant Steels (Woodhead Publishing Series in Metals and Surface Engineering). 1st ed. England: Woodhead Publishing; 2008

[103] Rusinko A, Rusinko K. Plasticity and Creep of Metals. Chennai, India: Springer; 2011

[104] Hyde TH, Sun W, Hyde CJ. Applied Creep Mechanics. NewYork, NY: McGraw-Hill Education; 2014

[105] Kasnner ME. Fundamentals of Creep in Metals and Alloys. 3rd ed. Amsterdam, The Netherlands: Butterworth Heinemann is an imprint of Elsevier; 2015

[106] Lokoshchenko AM. Creep and Creep Rupture of Metals. 1st ed. England: CRC Press; 2017

[107] Charit I, Zhu YT. Mechanical and creep behavior of advanced materials: A SMD Symposium Honoring Professor K. Linga Murty. The Minerals, Metals & Materials Series, Springer; 1st ed. 2017